# CHAPTER 1

# Introduction

***"For dust you are and to dust you will return."***

***– Genesis 3:19***

## 1.1 Cosmic Dust

The term "cosmic dust" refers to very tiny particles comprised of heavy elements (such as O, C, Si, Mg, Fe) that exist in the interstellar medium (ISM). Although very different in composition and properties from the everyday dust we find in our households, cosmic dust regulates the way we perceive the universe around us. Interestingly, cosmic dust was considered to be an obstacle by early optical astronomers since it absorbs and scatters incoming radiation and blocks our view of an object, hence making it appear dark. However, with the advent of telescopes operating in the infrared part of the electromagnetic spectrum, it became known that the absorbed shorter wavelength visible light is, in fact, re-radiated by dust at longer wavelengths. Thus began an era encompassing new discoveries of hitherto dark and hidden parts of the universe.

In spite of ample variation in the particle size ranging from a few molecules to a few microns, 'dust grains' still maintain a continuity in their physics, which makes them a bridge between understanding the behaviour of microscopic particles and how they are able to affect macroscopic events occurring at galactic scales [1]. The role of dust in the birth and death of stars has become a key element in understanding the formation of various astrophysical objects including planets like our Earth. It is now known that dust particles, albeit being negligible in mass ($\sim$1% of ISM mass), act both as a heat source and a coolant in the interstellar as well as the intergalactic medium ([2, 3], and references therein). Most importantly, dust provides a site for molecules to form, including hydrogen ($H_2$) which is the basic building block essential for sustenance of life forms. Dust studies have therefore become a powerful tool to study not only important astronomical, astrophysical and astrochemical phenomenon, but the origin of life itself in the universe around us.

### 1.1.1 Origin and evolution

The dust particles found in the interstellar medium (ISM) are generally referred to as 'stardust' due to the existence of substantial evidence that dust grains form as a result of condensation in stellar outflows consisting of rapidly-cooling gas [4, 5]. Infrared emission has been observed from dust in the outflows from asymptotic giant branch (AGB) stars, red giants, supernovae (SNe) and Wolf-Rayet stars among others [6]. In fact, AGB stars are thought to be the primary source of stardust in our Milky Way and both the neighbouring Magellanic clouds [6–8]. However, since the typical time for stars to attain the AGB phase is ∼1 Gyr, the notable contribution to stardust in the early universe was from massive SNe in contrast to the current scenario where Sun-like stars have a much more significant contribution towards the production of stardust ([2] and references therein). The first observations of stardust contributed by SNe were much larger than theoretically expected which had led to an uncertainty in the amount of stardust originating in SNe. Nevertheless, more recent observations of SNe by the *Spitzer* and *AKARI* space telescopes in the infrared along with other observations in the sub-millimetre have concurred with the expected 0.01–0.1 $M_\odot$ contribution by individual SNe [9–11]. Therefore, the bulk of the dust grain mass comes from circumstellar shells in the vicinity of evolved stars. Figure 1.1 shows a schematic diagram of the cosmic dust life cycle.

Once the stardust moves away from the stellar outflows and into the ISM, they face various interstellar processes which lead to dust grain destruction and evolution. Such processes include sputtering due to bombardment by protons in hot gas which leads to grain erosion [12, 13]. In addition, stardust may get shattered or vaporized during grain-grain collisions induced by interstellar SNe shock waves [1, 2]. Moreover, high energetic ultraviolet (UV) or cosmic ray/X-ray radiation may cause photolysis and alteration of dust grains. Therefore, despite the fact that dust is formed during stellar outflows, most of the dust in the ISM is not stardust. The dust grains get processed in the ISM which alters their composition and properties. Now, stardust gets injected into the ISM over a time period ∼1 Gyr [6], but the theoretically predicted dust grain lifetime in the ISM, taking into account the destruction efficiency, is ∼100 Myr [14–16]. So, in order to account for the dust abundance still found in the ISM, there must be some additional mechanism for their production.

The depletion of stardust from the ISM due to their destruction is balanced by the dust grain production in the ISM itself [7, 15]. The growth of dust grains in the ISM happens due to the accretion of atoms and molecules on top of pre-

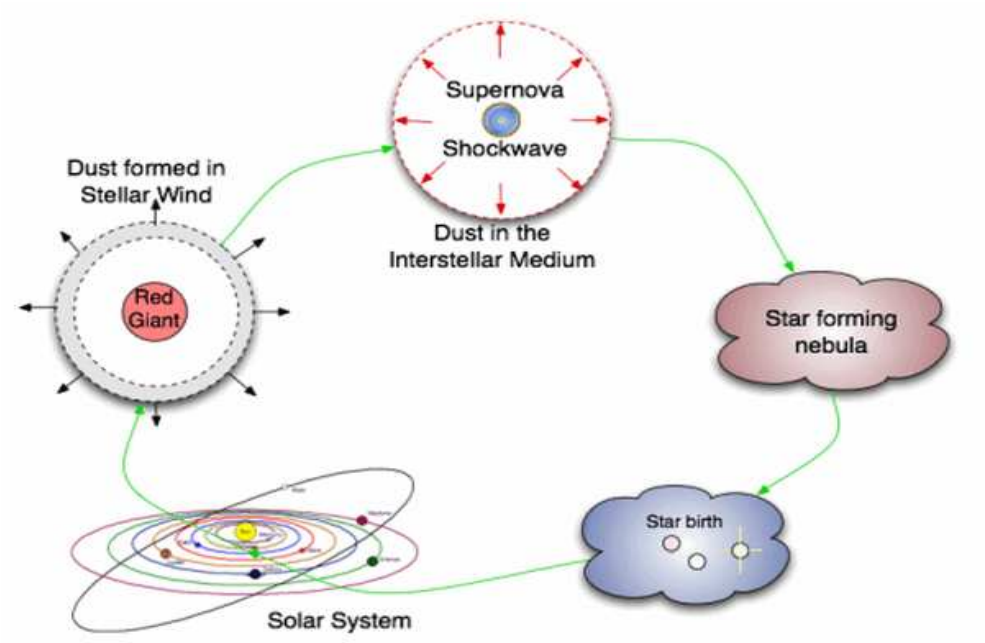


*Figure 1.1:* A schematic representation of the cosmic dust life cycle. Image taken from the *Hershel Space Observatory* website: http://herschel.cf.ac.uk/science/infrared/dust

existing grains in dense molecular clouds which may even lead to a change from gaseous to the solid phase. This causes an increase in the ISM dust mass and such growth can also explain the reduction of elemental abundance in the gaseous phase of the ISM [2]. Hence, there exists a balance between the destruction of dust grains by SNe shocks and the dust growth due to accretion processes.

### 1.1.2 Extinction and reddening

The reddening of starlight coming from distant stars due to tiny particles present in the ISM was discovered over 80 years back [17]. This acted as concrete evidence in support of the existence of interstellar dust which absorbs the incident radiation at short wavelengths and re-radiates more than 30% of it in the longer infrared [1, 18]. In addition, dust grains cause substantial scattering of radiation at visible and ultraviolet wavelengths which are used as a tool to study the optical properties of dust grains such as albedo and scattering phase function which is dependent on the angle of scattering [1]. The phenomenon of scattering and absorption caused by dust grains is collectively known as dust 'extinction'. This attenuation is highly wavelength-dependent and has a higher tendency of occurring at shorter (blue) wavelengths rather than longer (red), which is why it is often termed as reddening.

The need to correct for the effects of extinction by interstellar dust on incident radiation has, therefore, become highly crucial in order to determine the intrinsic properties of any astrophysical object accurately. It is often assumed that extinction is negligible at very long wavelengths and this helps us to ascertain the value of extinction towards a star using the 'pair method'. Considering two stars such that one is heavily reddened and the other has negligible amounts of foreground dust, a comparison of their spectrophotometry allows us to precisely determine the extinction, provided both stars fall in the same spectral class [1]. This method has been successfully used to measure the wavelength-dependent extinction along different sightlines which is represented by an 'extinction curve' across a range of wavelengths ranging from the ultraviolet (UV) to the mid-infrared (MIR). These extinction curves are the primary source for information on dust grain properties in the ISM of different galaxies [7]. The ratio of total to selective extinction, represented by $R_V = A_V/(A_B - A_V)$, is used as a measure of the extinction curve slope in the visible region. A value of $R_V \to \infty$ indicates the presence of very large grains and an $R_V \approx 1.2$ would indicate Rayleigh scattering, i.e. by dust grains much smaller than wavelength. Hence, larger values of $R_V$ would mean a possibility of grain growth towards that sightline [1]. For the Milky Way, the average extinction calculated along different sightlines using the pair method reveals an $R_V = 3.1$ [19, 20]. The extinction curves for the Milky Way ($R_V = 3.1$) and the Magellanic clouds are shown in Figure 1.2 [21].

The interstellar extinction curves for the Milky Way (MW), the Large Magellanic Cloud (LMC) and the Small Magellanic Cloud (SMC) have been measured extensively along many lines of sight to study the extinction, which also depends on dust grain structure and composition [22]. Although similar in the tendency to rise from the infrared towards the ultraviolet, the average extinction curves show significant changes among the MW, LMC and SMC. The most distinct difference among the three is in the peak of the 2175 Å feature which decreases from the MW to the LMC and is almost absent towards some particular sightlines in the SMC, as seen in Figure 1.2 [21]. It is believed that this feature is caused due to an electronic transition in graphite particles or molecules of polycyclic aromatic hydrocarbon (PAH) [23]. The observed extinction curves in the MW and the LMC have been reproduced using appropriate mixtures of silicates and some form of carbon while the extinction curve for the SMC bar can be reproduced using silicates alone [24, 25]. Moreover, it has been observed that the extinction in the UV decreases from the MW to the LMC to the SMC which is indicative of variations in the dust grain

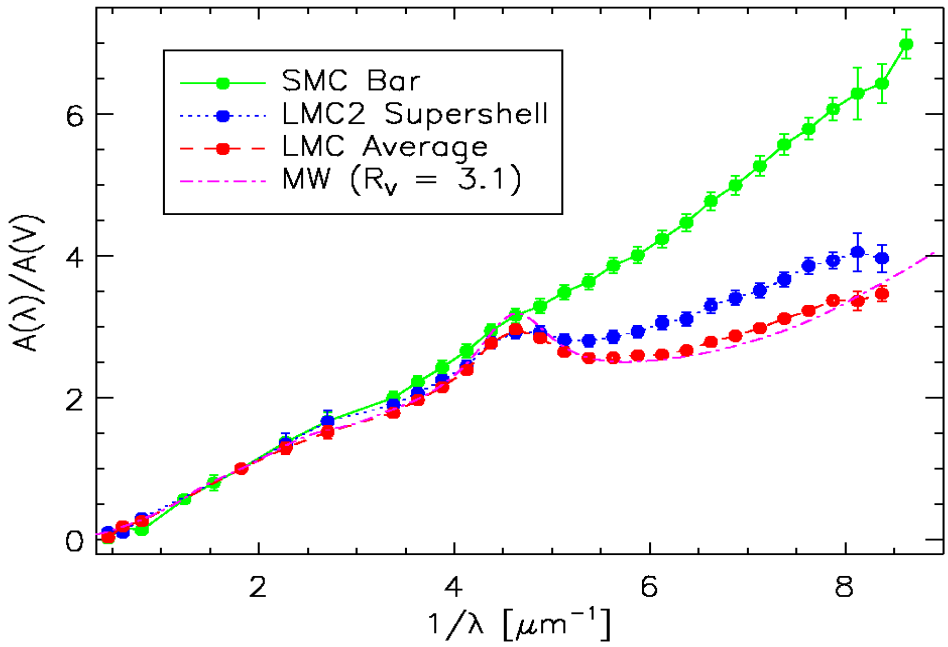


*Figure 1.2:* The average Milky Way and Magellanic cloud extinction curves. Reproduced from Gordon et al. (2003) [21] under the Creative Commons Attribution-ShareAlike 3.0 Unported license: https://creativecommons.org/licenses/by-sa/3.0/

size and/or composition, with a lower value of $R_V$ analogous to abundance of smaller sized grains [26]. It is also seen that there is a decrease in metallicity (abundance of elements other than hydrogen and helium) in the order: $MW > LMC > SMC$ as the fraction of smaller grain size increases [3].

The Magellanic clouds have a lower metallicity as compared to the MW which makes them an ideal, nearby laboratory for extragalactic dust studies. The LMC and SMC have metallicities similar to galaxies found at high redshifts which makes them valuable for probing the interstellar dust properties in distant galaxies. Of course, the level of attenuation by dust can vary strongly from one galaxy to another depending on the sightline [3]. Nonetheless, the observed extinction curves, when compared with theoretical dust models, still provide ample knowledge regarding the properties of dust grains in the ISM.

### 1.1.3 Grain properties

#### Composition

As mentioned in the previous section, the primary source of information on dust grain composition comes from the emission and/or absorption features in the observed extinction curve. The prominent spectral features used to constrain the material composition of dust grains are discussed here.

**2175 Å feature:** It was first brought to attention by Stecher & Donn (1965) [27] that the 2175 Å feature could be produced by small particles of graphite. Since then, although various carriers among the most abundant elements found in the ISM (C, O, Mg, Si, Fe) have been proposed as being responsible for this feature, it has been found that graphitic carbon in some form is the component responsible for the 2175 Å peak [1]. It has also been observed that the electronic transition in the carbon atom frame of graphite, which is responsible for the occurrence of the 2175 Å feature, is similar to what is produced by PAH molecules in the 2000-2500 Å spectral range [25, 28]. Therefore, PAHs have been incorporated into various dust models in order to explain the occurrence of this feature as a continuation of the graphite based model [26].

**Silicate features:** In addition to the 2175 Å feature in the UV, the interstellar extinction curve shows an absorption feature around 9.7 $\mu$m due to stretching of the Si-O bond. Such a 10 $\mu$m feature is also observed in the emission outflows from cool stars rich in oxygen where silicate production occurs. On the other hand, AGB stars rich in carbon produce silicon carbide (SiC) where the oxygen is bonded as CO. This is seen as an emission feature at 11.3 $\mu$m in meteorites and carbon stars [29, 30]. Now, the broad 9.7 $\mu$m feature is in contrary to the sharp peak shown by crystalline silicates in the laboratory which suggests that silicates in the ISM are predominantly amorphous in nature. Moreover, there is another feature due to bending in the O-Si-O bond which is observed at 18 $\mu$m. It has also been argued that silicate grains tend to be fluffy and porous which is necessary to reproduce the observed silicate features ([26] and references therein). Although silicates are not found abundantly in crystalline form, there have been recent evidences which put a limit to the amount of crystalline silicates in the ISM, e.g. $\sim$2% by Kemper et al. (2004, 2005) [31, 32] and $\sim$1% by Min et al. (2007) [33]. In contrast, crystalline silicates which are mostly rich in Mg have been observed frequently in protoplanetary disks around young stars ([34] and references therein).

**PAH features:** The strong emission features shown by many reflection and emission nebulae in the 3-15 $\mu$m range have been attributed to the presence of PAH molecules. Such emission, which is mainly seen at 3.3, 6.2, 7.7, 8.6 and 11.3 $\mu$m, is much stronger than what is expected from thermal heating of dust grains and actually happens due to the different vibrational modes which are optically active in PAH molecules [35, 36]. The PAH abundance in the MW is such that it contributes to $\sim$5% of the grain mass and $\sim$20% of the infrared emission and starlight absorption. It has been observed that smaller

PAH grains radiate at shorter wavelengths while larger PAHs show emission towards longer wavelengths ([26] and references therein).

**Others:** In addition to the occurrence of oxides such as silicates in oxygen-rich regions, ices containing oxygen are also expected to be formed. The ices tend to condense on top of existing dust grains and the detection of ices such as CO, $CO_2$, $H_2O$ and $CH_3OH$ has been reported in molecular clouds [37]. On the other hand, material such as sulfides and carbides are formed towards carbon-rich regions [34]. Furthermore, there could be heterogeneous compositions as well, e.g. silicates with iron coating, graphites with silicate coating, etc. but such cases have not been studied well [2].

### Size distribution

We now know that dust grains which contribute to the infrared emission in the ISM are very small in size, ranging from few tens of atoms to hundreds of them. Since the extinction curve is the primary information source for dust grain properties, Mathis, Rumpl & Nordsieck (1977) [38] used a mixture of spheres consisting of graphites and silicates to reproduce the observed extinction curve from the UV to near-IR. They used a non-parametric approach to best-fit the size distribution using limits on the grain size, $a_{min}$ and $a_{max}$, and found a power-law distribution with $a_{min}$ $\approx$0.005 $\mu$m and $a_{max}$ $\approx$0.25 $\mu$m as the best fits. This is famously known as the "MRN" size distribution. However, the MRN distribution did not take into account the presence of PAHs which are now known to account for $\sim$5% of the ISM grain mass and are substantial contributors to the extinction observed in the UV.

More recent dust models [25, 39, 40] have taken into account the contributions of PAHs in addition to carbonaceous and silicate dust in order to fit the extinction using various size distributions. Although it has been observed that a wide range of dust grain sizes are needed to reproduce the rise in the extinction curve from IR to UV, $\sim$50% of the ISM dust mass comes from grain sizes below $\sim$0.1 $\mu$m [26]. The general consensus is that dust grains with sizes in the range 0.05 $\mu$m$< a <$0.3 $\mu$m are required to produce extinction in the visible range of the electromagnetic spectrum in the ISM. However, various processes in the ISM are likely to modify the grain size distribution with an overall balance between grain coagulation and dust grain destruction by collisions [41, 42]. In fact, the sub-micron sized dust grains can come together in dense regions of the ISM such as circumstellar disks and envelopes, dense molecular clouds, etc. and form larger sized particles

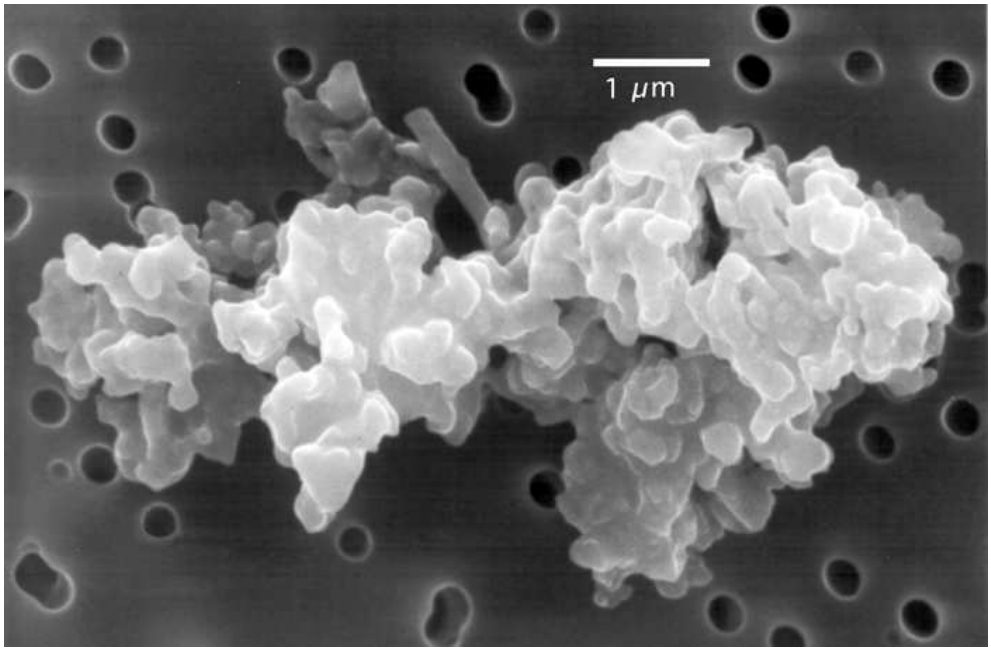


*Figure 1.3:* An interplanetary dust particle formed by accumulation of a number of sub-micron sized dust grains as seen with a scanning electron microscope. Reproduced from Jessberger et al. (2001) [43] under the Creative Commons Attribution 2.5 License: https://creativecommons.org/licenses/by/2.5/

[34]. An interplanetary dust particle which is porous in nature and formed by accumulation of a number of sub-micron sized dust grains is shown in Figure 1.3 [43]. Hence, the total size distribution is efficiently estimated not only using the UV-optical extinction curve of the ISM, but also from emissions in the IR complemented with measurements of elemental depletions from the ISM [35, 44–46].

### Polarization

Polarization in the ISM is caused by the alignment of asymmetric dust grains in response to the magnetic field [47] and it was first observed over 60 years back at visible wavelengths due to dichroic extinction of incident starlight [48, 49]. It has now been observed in the UV [50], near-IR [51] as well as in far-IR emissions [52, 53] along various sources and sightlines. Therefore, just like dust grain properties can be derived on the basis of the wavelength-dependent extinction curve, the composition, size and spatial distribution of aligned dust grains can be estimated using the polarization curve which is also wavelength-dependent [40, 54–56]. Spectropolarimetry can be used in conjugation with the polarization profile to obtain additional information such as the dielectric function of a material which we cannot get by studying just the intensity profile. For example, the two prominent silicate features can also be observed

in polarization either in case of emission or absorption but while the 9.7 $\mu$m feature is consistent with the dielectric function of 'astronomical silicates' [57], the observed polarization is stronger than what is expected around the 18 $\mu$m feature for silicates with the same dielectric function [58, 59].

The incoming starlight which is scattered by dust grains gets partially polarized and the resulting linear polarization fraction is most efficient in the UV [60]. In addition, the background light passing through elongated, aligned dust grains residing in a molecular cloud also gets partially polarized due to the presence of a magnetic field [3]. The polarization produced by this process in the Milky Way follows the Serkowski law [61]. It is effective from the near-UV to the near-IR and peaks around $\lambda_{max}$ $\sim$0.55 $\mu$m, which when considered under the Rayleigh approximation ($2\pi a/\lambda$)$\approx$1, gives us a grain size, a$\approx$0.1 $\mu$m. Hence, the larger sized 'classical' grains (extremes at 0.1 $\mu$m and 0.5 $\mu$m) give the most contribution towards polarization in the ISM as smaller sized grains ($\sim$0.05 $\mu$m) generally do not get aligned as a response to starlight torques [26, 55]. The observed polarization also confirms that the dust grains responsible are irregular and non-spherically shaped. The extinction cross sections of such grains can be generated using various approximation techniques such as the Effective Medium Approximation (EMA) based on the Mie theory and the Discrete Dipole Approximation (DDA) which will be discussed in details in Section 1.3.3.

### 1.1.4 Overview of dust models

The interaction of electromagnetic radiation with dust grains which causes extinction, polarization, reflection and re-emission of starlight is our principal source of information on the nature and properties of cosmic dust. However, the deduction of these dust properties is not straightforward and cannot be directly measured. Hence, we take the help of tentative dust models which mimic the geometry, composition, size and other dust grain properties. We then compare the model predictions with actual observations of interstellar extinction, polarization and so on to constrain the grain properties. An ideal dust model should allow the user to specify potential candidates for grain material, be it real ones studied in the lab (e.g. SiC, graphites) or some alternatives for lesser know materials found in the ISM (e.g. astro-PAHs, astro-silicates). It should also offer provisions to specify the shape and size distribution of grains, with an ability to effectively calculate the scattering and absorption cross sections of the dust grains in the model [23, 26, 62].

In the past 40 years, various grain models have been proposed to constrain the properties of interstellar dust. An extensive review of all these dust models is given by Draine (2004) [62] who has divided them into three categories broadly: (1) the original silicate and graphite based model [38, 57, 63] which was later extended to incorporate PAHs as well [25, 28, 64]; (2) models which assume dust grains to have a carbonaceous mantle over a core made of silicates [45, 65, 66]; and (3) the composite dust grain model which expects dust grains to be comprised of aggregates of carbonaceous particles and silicates [39, 67, 68]. All these models were proposed before the advent of the *Spitzer Space Telescope* which was the largest space telescope operating in the mid and far-infrared during the time before the launch of *Hershel Space Observatory* in 2009.

More recently, in the post *Spitzer* era, Draine & Li (2007) [23] put forward an 'amorphous silicate–graphite–PAH' model with adjustments in composition to match the new *Spitzer* observations but with spherical grains. Compiegne et al. (2011) [46] proposed a "DUSTEM" model comprised of 'amorphous silicates–amorphous C–PAH' while Jones et al. (2013) [69] gave an 'amorphous silicate–Fe nano particle–amorphous C—PAH' model with similarly shaped spherical dust grains, none of which took dust grain polarization into account. With the advancements in polarimetric techniques, it is now possible to detect polarized emission from the diffuse ISM. Hence, an efficient dust model must be able to reproduce the polarization of starlight caused due to dust grain alignment. The prominent models in recent years which have considered spheroidal grains to predict the polarization produced during partial alignment are by Draine & Fraisse (2009) [40] with the same materials as Draine & Li (2007) [23] and the recent 'amorphous silicate–Fe–graphite–PAH' spheroidal grain model by Hensley & Draine (2015) [70]. Therefore, dust grain models which can make predictions regarding the degree of polarization in addition to predicting the dust grain extinction are the need of the hour.

## 1.2 Multi-wavelength observatories

In this thesis work, we have used the far-ultraviolet (FUV), mid-infrared (MIR) and far-infrared (FIR) observations made by different space-based telescopes to study the extinction and re-emission caused by dust grains. We have also used the MIR polarimetric observations made using a ground-based telescope to study the dust grain polarization. A brief overview of some of these observatories whose archival data has been used in our work is presented here.

### 1.2.1 Space-based

***Galaxy Evolution Explorer (GALEX)*** was launched by NASA in 2003 as a part of the Small Explorers (SMEX) program with a planned 29 month mission period. As the name suggests, *GALEX* explored the evolution and origin of galaxies and in addition, it also explored the origins of stars and heavy elements in the $0 < z < 2$ redshift range. The *GALEX* mission performed surveys of the UV sky in two wavelength bands: FUV ($\lambda_{eff}$ ~1528 Å, 1344–1786 Å) and near-UV ($\lambda_{eff}$ ~2310 Å, 1771–2831 Å) with different depth and coverage [71, 72]. *GALEX* had a field of view $\approx 1.2^0$ diameter, with a spatial resolution of $\approx 4.2''$ (FUV) and $\approx 5.3''$ (near-UV) [71]. The two detectors provided simultaneous observations of the same field in two bands owing to the presence of a dichroic beam splitter [73]. The *GALEX* all-sky imaging survey: AIS was completed in 2007 covering ~26,000 deg$^2$ [74]. It had the capability to detect a diffuse signal of 100 photons cm$^{-2}$ sr$^{-1}$ s$^{-1}$ Å$^{-1}$ in a typical AIS observation [75]. The mission operated till early 2012, extending three times it's originally planned period, while conducting all-sky imaging surveys, deep imaging surveys and a survey of 200 galaxies nearest to the Milky Way Galaxy in the ultraviolet (UV). We have used *GALEX* photometric data in the FUV for our work.

*Figure 1.4:* The *Galaxy Evolution Explorer (GALEX)* space telescope before being launched in 2003. Image credits: NASA/JPL.

***Spitzer Space Telescope (SST)*** was launched in 2003 as a part of the NASA Great Observatories program and served as an infrared counterpart to the *Hubble Space Telescope*. *Spitzer* used liquid helium to cryogenically cool the detectors in order to study the early universe, young galaxies and forming stars. It has also played an important role in planet formation studies by detecting dust disks around stars. The *SST* had three instruments on-board which were used for observations. We have used observations made by the two instruments having imaging capabilities. The Infrared Array Camera (IRAC) [76] was a four-channel infrared camera which provided simultaneous images at four wavelengths 3.6 $\mu$m, 4.5 $\mu$m, 5.8 $\mu$m and 8 $\mu$m. Each of the four detector arrays in the camera were 256×256 pixels in size, with a pixel size of 1.2×1.2 arcsecs. The Multiband Imaging Photometer for Spitzer (MIPS) [77] produced imaging and photometry in three broad spectral bands in the MIR and FIR: 128×128 pixels at 24 $\mu$m with a pixel size of 2.45×2.45 arcsec, 32×32 pixels at 70 $\mu$m with a pixel size of 4.0×4.0 arcsec, and 2×20 pixels at 160 $\mu$m with a pixel size of 8.0×8.0 arcsec. The Infrared Spectrograph (IRS) was used from low and high resolution mid-IR (5–40 $\mu$m) spectroscopy.

*Figure 1.5:* The *Spitzer Space Telescope* being assembled before launch in 2003. Image credits: NASA/JPL.

In July 2009, *Spitzer* ran out of it's supply of instrument-cooling liquid helium, switching to a "warm phase" and thus limiting it's study of super cold objects, but is still operational till date. We have mainly used the IRAC 8 $\mu$m and MIPS 24 $\mu$m archival data for our work.

***AKARI (ASTRO-F)*** was operated by JAXA from early 2006 till late 2011 with an aim to survey the entire sky in the infrared. The scientific goals of the *AKARI* mission were to understand the formation and evolution of galaxies, star formation, planetary formation and evolution. *AKARI* had two instruments on-board: the Infrared Camera (IRC) [78] and the Far-Infrared Surveyor (FIS) [79]. The IRC made observations using three independent camera systems: NIR (1.7 – 5.5 $\mu$m), MIR-S (5.8 – 14.1 $\mu$m) and MIR-L (12.4 – 26.5 $\mu$m). We have used MIR-L (12.4 – 26.5 $\mu$m) camera for 15 and 24 $\mu$m observations. One of the advantages of the IRC was it's ability to observe 10 square arcmins at a time because of large size detector arrays (512 $\times$ 412 pixels for NIR, 256 $\times$ 256 pixels for MIR). The FIS was the instrument chiefly intended to make an all-sky survey at FIR wavelengths [80, 81]. The FIS had effectively four observation bands: N60 (50 – 80 $\mu$m), WIDE-S (60 – 110 $\mu$m), WIDE-L (110 – 180 $\mu$m) and N160 (140 – 180 $\mu$m). We have mainly used the FIS N60 and the FIS WIDE-S band archival data centered at 65 $\mu$m and 90 $\mu$m respectively, both with a pixel size of 26.8″ and an array format of 20×2 and 20×3 pixels respectively for our work.

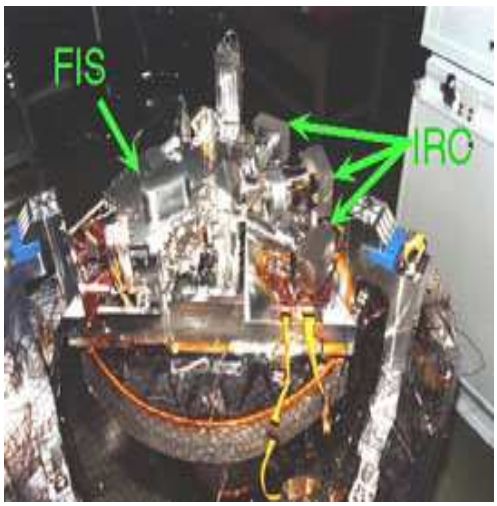


*Figure 1.6:* The scientific instruments on-board the *AKARI* space telescope. The FIS stands for Far-Infrared Surveyor and the IRC is the Infrared Camera operating in the near and mid-infrared. Image credits: JAXA.

### 1.2.2 Ground-based

There are a few polarimeters available today which operate at the optical as well as the near-IR wavelength bands. However, the number of polarimeters available at MIR wavelengths is surprisingly rare given the importance of the 8-13 $\mu$m band in understanding the dust re-emission and related properties. Even when there are MIR instruments available that do have polarimetric capabilities, they have been seen to make use of wire grid polarizers leading to reduced accuracy and lower observing efficiency as opposed to those that make use of dual-beam systems [82].

**CanariCam** is a high-resolution MIR imaging instrument (7.5-25 $\mu$m) mounted over the 10.4 metre reflecting telescope, Gran Telescopio Canarias (GTC), situated at La Palma, Spain [83]. It has spectroscopic, coronagraphic and polarimetric capabilities and has been constructed such that it reaches the telescope's diffraction limit at MIR wavelengths. CanariCam uses a Si:As based 320×240 detector with a field of view (FOV) ∼26″×19″. The advantage of using CanariCam is that it permits the use of a dual-beam polarimeter in the 10 $\mu$m window by inserting it in the optical path of a half-wave plate (HWP), a Wollaston prism and a field mask leading to an increased polarization efficiency (maximum ∼99.2% in the Si4-10.3 $\mu$m filter). Owing to some chromatic birefringence, the useful exposed field of view for CanariCam polarimeter is 320×25 pixels per slot (of the polarimeter mask) per polarized beam, which corresponds to 25.6″×2″. In the imaging polarimetry mode, more than 2.5 slots can be used, giving us a FOV of 25.6″×5″ [83].

## 1.3 Computational methods

In order to analyse the data observed by different telescopes, we have employed the help of some computational and statistical tools which we discuss here.

### 1.3.1 Aperture photometry

"Photometry" refers to measurement of the number of photons in the electromagnetic radiation coming from an astronomical source, which is represented in terms of flux or intensity at a particular wavelength. It essentially tells us the brightness of an object which has been observed by the photometric detectors on-board a telescope.

Aperture photometry, as the name suggests, involves the use of an aperture (circular, elliptical, square, etc.) of sufficient size which is overlaid on an image with the object/source as center, followed by summing up of all the pixel counts within the aperture to get the flux/intensity value. However, this value has a contribution from the "sky background" in addition to the source which needs to be subtracted in order to isolate the true flux from the source alone. Hence, a larger sized aperture is used which forms an annulus as shown in Figure 1.7, with the assumption of a constant sky background value all over the aperture. The average sky background value is then subtracted from the summed up pixel counts centered on the source within the aperture, giving us the sky-corrected flux/intensity of an object [84].

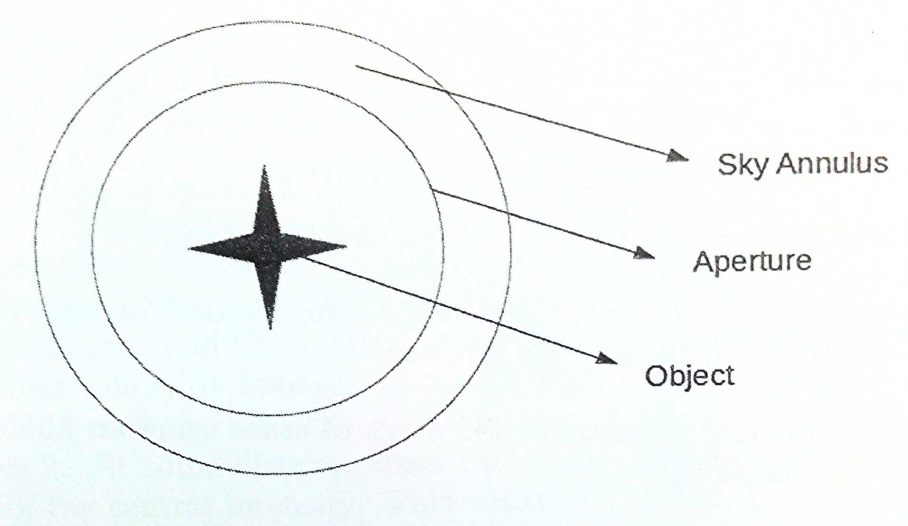


*Figure 1.7:* Aperture photometry of a point source/object using a sky annulus to correct for the effects of background contamination.

In case of point sources, the aperture photometry technique is carried out using various software tools [85], e.g. PhotUtils package in Python, APER function in IDL, qphot package in IRAF and so on. However, the aperture photometry in case of diffuse sources, such as the ones we have studied throughout this thesis work, is not so straightforward due to the lack of a point source which makes it difficult to determine the size of the aperture to be used. More importantly, it becomes very difficult to differentiate between a diffuse source and the sky background. Hence, we have used the aperture size of the particular telescope detector which was used to obtain the photometric data/images and then calculated the median value of pixel intensity within the aperture in order to determine the flux/intensity centered on a diffuse location.

Moreover, all the photometric data which has been used in our work has already been calibrated and corrected for sky background, i.e. we have used the post basic calibrated data (pbcd) products from the telescope archives.

For example, in case of *Spitzer* IRAC, a median background is computed for the whole frame which is then subtracted while for *Spitzer* MIPS, the data is reduced using the SSC model which gives the the Cosmic Infrared Background (CIB), ISM and zodiacal light contributions. The details of background estimation and removal in both cases can be found in the IRAC and MIPS instrument handbooks available in the NASA/IPAC infrared science archive. The calibration details for AKARI FIS can be found in Takita et al. (2015) [81] and the AKARI FIS data user manual [86].

### 1.3.2 Correlation studies

We have used the Spearman's rank correlation coefficient ($\rho$) which is a simple and reliable method to test both the strength and direction (positive or negative) of the monotonic relationship between two variables rather than the linear relationship between them [87]. It does not assume any model, like a straight line fit, and hence it is non-parametric. We have used Spearman's rank correlation because monotonicity is 'less restrictive' than that of a linear relationship, i.e. we might get a pattern among our observed data that is monotonic, but not linear, and so it still tells us that they are related [88]. It also has the advantage of being less sensitive to bias which might come in due to the effect of outliers in the data set. The Spearman's rank correlation coefficient is calculated by first converting the observed values to ranks and then using the following relation:

$$\rho = 1 - \frac{6\Sigma d^2}{n^3 - n} \tag{1.1}$$

where, $\Sigma$ = sum, d = difference between two ranks, n = no. of pairs of data.

The rank correlation coefficient, $\rho$, can take values inside the interval [-1, 1]. A value of +1 indicates a perfect association of ranks (as the value of one variable increases, so does the value of the other variable), zero indicates no association between ranks (no relation between the variables) and -1 indicates a perfect negative association of ranks (as the value of one variable increases, the other variable value decreases). The closer $\rho$ is to zero, the weaker the association between the ranks.

Once we have calculated the rank correlation, we must test to see how likely it is that our calculation is not just the result of chance which is called significance testing and is given by a 'p-value'. It considers our result in relation to how much data we have. A small p-value indicates strong

evidence against the null hypothesis (typically <0.05), so one can reject the null hypothesis and a large p-value indicates weak evidence against the null hypothesis. Hence, lower the p-value, more is the reliability in the observed rank correlation coefficient value.

### 1.3.3 Extinction calculations

The starlight scattered/reflected by dust gives us information regarding the optical properties of the grains involved. The dust grain 'albedo' gives us an estimate of the fraction of incident radiation which gets scattered and the asymmetry factor (g) tells us the direction and nature of scattering. A combination of these two ($\alpha$, g) can be used in models for comparison with observations to determine the extinction caused by dust grains in a region. We have used the dust model by Shalima et al. (2006) [89] which constrains the albedo and asymmetry factor of dust grains using the Henyey–Greenstein scattering phase function [90]:

$$\phi(\theta) = \frac{(1-g^2)}{4\pi[1+g^2-2gcos(\theta)]^{\frac{3}{2}}} \tag{1.2}$$

where 'g' is the phase function asymmetry factor and $\theta$ is the scattering angle. A value of g close to zero implies that the scattering is nearly isotropic while a value of g near 1 implies strongly forward scattering grains. A negative g value implies backscattering by dust grains which we cannot observe.

Various studies have identified dust grains to be porous and fluffy in nature, occurring as conglomerates comprising of multiple very tiny grains attached together due to collisions or interaction among the grains and various other processes which are likely to make the dust grains non-spherical and inhomogeneous ([91] and references therein). The interaction between such dust aggregates and the incident electromagnetic radiation can be studied using a 'deterministic approach' to solve Maxwell's equations in frequency domain for individual clusters. However, such exact methods can only be used for small systems showing moderate absorption, mainly due to computational limitations [34]. Hence, in the absence of a precise theory for the study of highly absorbing dust grains, we take the help of various approximation techniques, e.g. the EMA: Effective Medium Approximation and the DDA: Discrete Dipole Approximation, to model the extinction caused by such grains.

The EMA method [92] uses T-Matrix which is based on Mie theory in order to determine the optical properties of small composite particles which

may be either spherical or non-spherical in nature. However, in case the particle is inhomogeneous, EMA replaces it by a homogeneous particle with a single averaged optical property (refractive index, dielectric constant) which is also it's limitation [93–95]. On the other hand, DDA [96] is more computationally precise and works very well for inhomogeneous particles taking into consideration the effects of various irregularities (shape, surface roughness, internal structure of grains). DDA represents an arbitrarily shaped composite dust grain in an array form with dipole elements which will experience a polarization whenever an electromagnetic radiation is incident and also due to oscillation of the rest of the dipoles. The interaction and superposition of these two polarization components causes scattering cross sections and extinction [97].

In spite of the drawbacks of the EMA T-Matrix method, it is very convenient for large size parameters and large complex refractive index where DDA poses a computational challenge. In addition, EMA also allows the user to explore the suitability of various dust mixtures [98, 99]. Both these approximation methods have been used recently in a work by Gupta et al. (2016) [91] to study the dust grain absorption using composite grain models and we have used a similar approach to study the polarization produced by spheroidal dust grains around young stars.

## 1.4 Objectives and Thesis outline

The aim of this thesis work, as the title suggests, is to study the characteristics of dust grains found in the Milky Way and nearby galaxies, with a special interest towards dust in the Magellanic clouds.

The first half of this thesis presents multi-wavelength correlation studies which have been used to identify the particular grain population responsible for the observed emissions. In **Chapter 2**, we have studied the FUV-IR rank correlation coefficients in the Milky Way (MW) by separating our observations into low and high latitude locations. We have proposed an extragalactic origin of dust for the observed emissions at high latitude locations in the MW [100]. We look beyond our Galaxy in **Chapter 3** where we have studied the correlations in the diffuse ISM of the Large Magellanic Cloud (LMC). We present our findings for two HII regions, namely N11 and 30 Doradus in the LMC [101]. As mentioned earlier, the Magellanic clouds have long served as ideal nearby laboratories to study dust properties and abundances in high-redshift galaxies owing to their nearly face-on orientation and closeness to the MW.

The Small Magellanic Cloud (SMC), with its unique properties as evident from the interstellar extinction curve, has been very interesting for the study of dust properties in galaxies which are in the early stages of their chemical enrichment. In **Chapter 4**, we probe the low-metallicity regions of the SMC using UV-IR correlation studies with an aim to provide a suitable justification for the absence of the 2175 Å feature by studying the PAH abundance in the SMC.

The second half of the thesis is focussed towards dust grain models to study the extinction in our local universe. In **Chapter 5**, we have used the Orion nebula as our sample of study to investigate the optical properties of dust grains in the MW. We complement the inferences drawn from correlation studies with a model to study the scattering caused by dust grains present in the ISM between us and Orion's veil. We present the dust grain albedo, asymmetry factor and the distance to individual dust locations in our line of sight [102]. In **Chapter 6**, we have investigated the polarization caused by dust grains around young stars using composite dust grain models. We have compared the results from our DDA and EMA approximation based models with actual observed polarimetric data in an attempt to constrain the dust grain composition and properties in our sample of stars.

We have compiled the important conclusions from each work and presented them together in **Chapter 7**. The thesis concludes with a brief summary and prospects for future work as presented in **Chapter 8**.